



Effect of formic acid (HCOOH) on the corrosion protectiveness of magnetite (Fe₃O₄) at elevated temperature

Maryam Eslami^{a,1}, Yoon-Seok Choi^{a,*}, Srdjan Nescic^a, Robert Breining^b

^a Institute for Corrosion and Multiphase Technology, Department of Chemical and Biomolecular Engineering, Ohio University, Athens, OH 45701, United States

^b Air Liquide Global E&C Solutions Germany GmbH, 60439 Frankfurt am Main, Germany

ARTICLE INFO

Keywords:

Sweet corrosion
Sour corrosion
High temperature corrosion
Formic acid
Corrosion product
Magnetite

ABSTRACT

The corrosion behavior of carbon steel in an aqueous solution containing dissolved CO₂, H₂S, and HCOOH at high temperature was investigated by conducting a series of systematic experiments. The influence of each (possible) corrosive species (CO₂, H₂S, and HCOOH) on corrosion mechanisms were explored through detailed analysis of corrosion rates and corrosion product layers. The results showed that the formation and integrity of the Fe₃O₄ layer was compromised in the presence of HCOOH, probably due to the formation of Fe(COOH)⁺ which impedes the formation of Fe₃O₄ at the initial stage of the corrosion process.

1. Introduction

Gasification process involves a multicomponent gaseous environment which typically includes a mixture of CO, CO₂, H₂, H₂O, CH₄, H₂S, Ar, N₂, COS, and HCN₃ [1–4]. The presence of CO₂, and H₂S makes this environment corrosive for many candidate materials such as carbon steel and stainless steel [5–8]. Beside the mentioned chemicals, the presence of organic acids such as acetic acid (CH₃COOH) and formic acid (HCOOH) has been reported in some gasification plants for feedstock of residue from conventional sources. However, little attention has been given to their role in the corrosion behavior of carbon steels and low alloy steels exposed to such environments. Alongside the critical corrosive environment, the temperature of piping and equipment in different locations of a gasification plant varies from 150 °C to 400 °C (this range can be different in various types of gasification plants and higher for biomass plants. The range given is specific for the targeted plant in the current study) [9,10]. Such high temperatures make the corrosion of service materials even more crucial.

One of the most important factors determining the corrosion kinetics and mechanism under such complicated and critical conditions is the type of corrosion product (e.g. carbonates, sulfides, oxides) that forms during the process [11]. However, corrosion studies focusing on layer formation under such a complicated environment are rare and, to the best of our knowledge, none of them cover the effect of organic acids [1,

2,4,9,10,12]. Nevertheless, related information can be also derived from the available literature on high temperature CO₂ and H₂S corrosion.

According to the study by Yin *et al.* [13], the thickness of the corrosion product layer formed under high CO₂ pressure (4 MPa) in chloride salts containing electrolyte decreased with temperature from 50 °C to 180 °C and a two-layered structure of corrosion products, including a “thick, porous, and loose layer” on top and a “thin, dense, and adherent layer” formed on the steel surface. The compactness of the corrosion product layers increased at higher temperatures. However, the corrosion rates did not match the SEM observation as the lowest corrosion rate was recorded at 100 °C and not at higher temperatures (i. e. 150 °C or 180 °C). Unfortunately, the phase characterization was only provided for the corrosion product layer formed at 70 °C, which showed that this layer contained iron carbonate (FeCO₃). Nevertheless, it is obvious that temperature has a determining effect on the corrosion rate and the formation of corrosion products. Tanupabrungsun *et al.* [14] observed a decrease in corrosion rate with increasing the temperature from 80 °C to 250 °C during their CO₂ corrosion experiments. This decrease was attributed to the nature of the corrosion product formed at different temperatures. According to X-ray diffraction (XRD) analysis at 80–150 °C, FeCO₃ and Fe₂(OH)₂CO₃ were formed on the steel surface. While at 200–250 °C, the corrosion product was exclusively Fe₃O₄. This implies that Fe₃O₄ provides superior corrosion protection compared to FeCO₃. Similar results were observed by other researchers showing the

* Corresponding author.

E-mail address: choiy@ohio.edu (Y.-S. Choi).

¹ Present affiliation: Applied Research Institute, The Grainger College of Engineering, University of Illinois Urbana-Champaign, Champaign, IL 61820, United States.

<https://doi.org/10.1016/j.corsci.2024.111868>

Received 19 December 2023; Received in revised form 18 January 2024; Accepted 20 January 2024

Available online 23 January 2024

0010-938X/© 2024 Elsevier Ltd. All rights reserved.

significant protection provided by Fe_3O_4 [11,15,16]. Hua *et al.* [16] reported a decrease in general and localized CO_2 corrosion rates with the temperature increase from 90 °C to 250 °C. In this case this decrease was also attributed to the conversion of the corrosion product layer from $FeCO_3$ to Fe_3O_4 .

Formation of Fe_3O_4 has been noticed in sour (H_2S) [17,18] and CO_2/H_2S environments as well. Ramanarayanan *et al.* [19] reported the formation of double-layered corrosion product in an $Ar - 10\%H_2S - (5 - 80)\%CO_2$ environment at 220 °C, in which an inner fine-grained layer with small amounts of magnetite in a pyrrhotite matrix and a thicker outer layer of pyrrhotite ($Fe_{1-x}S$) was observed. Kvarckval *et al.* [20] also observed the formation of an inner iron oxide layer (with a thickness of 3–7 μm) underneath a top FeS layer (a mixture of mackinawite and pyrrhotite). However, neither of these two studies considered the effect of inner Fe_3O_4 layer on corrosion rate reduction to be significant when compared to that of FeS . The study by Gao *et al.* [21, 22] in a H_2S environment at high temperature (120 °C) was more focused on the formation mechanism of the inner oxide layer. They showed that under their experimental conditions, Fe_3O_4 was supersaturated almost immediately after Fe^{2+} ions were generated in the solution due to corrosion of the specimen. Therefore, Fe_3O_4 was expected to dominate the layer growth during the initial stage resulting in its formation as an inner layer [21]. However, their results also showed that Fe_3O_4 constantly converts to FeS (mackinawite) because it is more thermodynamically stable [22]. In terms of the influence on the corrosion, Fe_3O_4 was shown to be more effective than FeS in reducing the corrosion rate [21].

Back to the complex chemistry conditions in the environment of a gasification plant, other potentially corrosive chemicals that might influence the corrosion behavior and the formation of corrosion product are organic acids. Even though there are some studies on corrosion of stainless steel and mild steel in organic acid, such as CH_3COOH and $HCOOH$ [23–30], to the best of our knowledge, so far no experimentation has been conducted under corrosion product layer forming conditions in CO_2/H_2S environment to investigate the effect of $HCOOH$ (especially) at elevated temperatures. Nonetheless, two important pieces of information can be extracted from the available studies: 1- $HCOOH$ has been shown to be the most corrosive among other organic acids [26], 2- the corrosion rate in the presence of organic acids increases with temperature. While there are some indications about the influence of formate ($HCOO^-$) on the formation of protective corrosion product layers [29], none of available studies have come close to understanding the mechanism. In a recent study, the influence of CH_3COOH on the integrity and corrosion protectiveness by $FeCO_3$ layer was investigated [31]. It was revealed that under the experimental conditions of that research (3 wt% $NaCl$ solution at initial pH 6.3, 80 °C, and 0.053 MPa pCO_2 , supersaturated with respect to $FeCO_3$), addition of undissociated CH_3COOH can result in the partial dissolution of $FeCO_3$ layer. This partial dissolution was explained by pH drop, an increase in the ionic strength of the solution and the formation of ferrous acetate complexes (such as $FeAc^+$ and $FeAc_2$) which all lead to a decrease in the $FeCO_3$ supersaturation.

In the present research, corrosion of carbon steel exposed to a complex gaseous system, that includes the potentially corrosive components of a gasification plant environment (CO_2 , H_2S , and $HCOOH$) and at the temperature representing the field condition was studied by means of electrochemical measurements and various surface analytical techniques.

2. Material and methods

ASTM A106 grade B carbon steel, with the chemical composition provided in Table 1, was machined into two different geometries: a cylindrical type with 5 cm² exposed area for the electrochemical measurements, and a rectangular type with a size of 2.5 cm × 1.3 cm × 0.3 cm for surface analysis.

Specimens were wet ground using 600-grit silicon carbide abrasive paper followed by rinsing in deionized (DI) water and isopropanol alcohol and drying with nitrogen (N_2) gas.

The high temperature experiments were carried out in a 7.5 L Hastelloy (C276) autoclave. A detailed schematic representation of this autoclave is shown in Fig. 1. A typical three electrode setup including a high pressure/temperature (HP/HT) $Ag/AgCl(0.1M KCl)$ reference electrode, the cylindrical steel specimen as the working electrode, and a platinum-coated niobium cylinder counter electrode were employed for the electrochemical measurements. A calibrated HP/HT ZrO_2 pH probe was used to monitor pH. A central impeller was used for stirring the electrolyte at the desired rotation speed during each experiment (1000 rpm \approx 1 m/s [32]). For the surface characterization, two rectangular specimens were immersed in the solution using the additional holders (with Teflon sample spacers) provided in the lid.

The testing conditions in the current research were selected from a process study based on the operational data. In the targeted plant, the highest temperature in the (simulated) loop results from a quenching step right after the gasification (where the formation of organic acids will occur) and this temperature was determined to be 237 °C. The equipment and piping will be subjected to vapors (with liquid films/droplets formed on the surface) or bulk liquids, depending on their

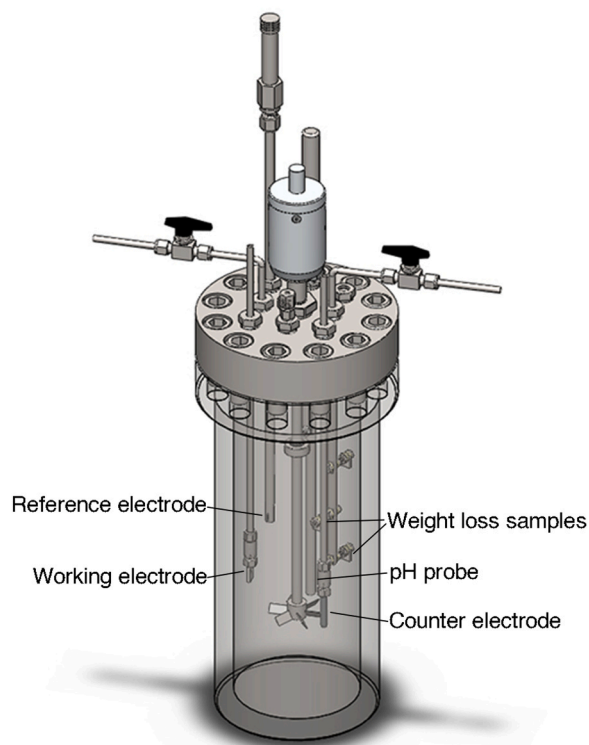


Fig. 1. Schematic representation of the autoclave setup.

Table 1

Chemical composition of carbon steel used in the present study (wt%, balance Fe).

C	Mn	P	S	Si	Cr	Ni	Mo	Cu	Al	V	Sn	Ti	As
0.24	0.74	0.01	0.006	0.25	0.09	0.06	0.03	0.16	0.03	0.0018	0.011	0.0016	0.007

position/pressure/temperature in the loop. Therefore, full immersion experiments as selected in this study represent the extreme case scenario.

The solutions for the experiments contained $HCOOH$ in addition to CO_2 and H_2S . To understand the effect of each of the (potentially) corrosive reagents, including H_2S and $HCOOH$, on the corrosion behavior and the formation of the corrosion product layers, different experiments were designed. In each experiment, one of the mentioned reagents was eliminated from the solution. The detailed conditions are presented in Table 2.

In order to achieve the same pH of 5.3 at the testing condition in each experiment, the required amount of $NaOH$ or HCl was calculated by using a water chemistry model [5], then the pH of the system was adjusted at the room temperature. For each test, the solution pH at 237 °C was measured to ensure achieving the target pH of 5.3.

For each experiment, 5 L of the solution was prepared with desired concentrations of $HCOOH$ (for experiments 1 and 2) or $NaCl$ (experiment 4) dissolved in deionized (DI) water. Experiment 3 was simply conducted in DI water without any of these reagents ($HCOOH$ or $NaCl$). The solution was de-aerated by continuous N_2 purging for a minimum of 4 h. Dissolved oxygen content in the solution was measured by an Orbisphere oxygen sensor after 4 h of N_2 purging and it showed concentration less than 5 ppb. The specimens were then placed into the lid, and the autoclave was sealed and heated to 80 °C while purging with N_2 . Due to safety considerations, the procedure was followed by pressurizing the system to a specific CO_2 and/or H_2S partial pressure at 80 °C instead of pressurizing it at the working temperature (237 °C). The required partial pressures of CO_2 and/or H_2S at 80 °C were calculated based on the premise that the total number of moles of CO_2/H_2S in the gas and the liquid phases are constant, hence the amount injected at 80 °C only into the gas phase was what would distribute between the gas and aqueous phases at higher temperature. After pressurizing at 80 °C, the system was heated up to the working temperature.

During each experiment, linear polarization resistance (LPR) measurements were conducted at regular time intervals (3 h) by polarizing the working electrode to the potentials of ± 10 mV with respect to open circuit potential (OCP) at a scan rate of 0.125 mV/s. The corrosion rate was then calculated as follows:

$$i_{corr} = \frac{\beta_a \cdot \beta_c}{2.3R_p \cdot (\beta_a + \beta_c)} = \frac{B}{R_p} \quad (1)$$

$$CR = 3.27 \times 10^{-3} \frac{EW \cdot i_{corr}}{\rho} \quad (2)$$

In Eq. (1), β_a and β_c are the anodic and cathodic Tafel slopes, and R_p is the measured polarization resistance (ohm.cm^2). The β_a and β_c were set at 40 mV/dec and 120 mV/dec, respectively, giving the B value of 13 mV. R_p was determined by the slope of the current voltage curve ($\frac{\partial E}{\partial i}$) at E_{oc} . In Eq. (2), i_{corr} is the corrosion current density ($\mu\text{A/cm}^2$), EW is the equivalent weight (g) and ρ is density (g/cm^3) of carbon steel.

Every experiment continued until a stable corrosion rate was reached. After each experiment, the specimens were removed from the autoclave, rinsed with DI water and isopropyl alcohol, dried with N_2 and stored in a desiccator in an inert atmosphere until surface analysis could be conducted. The surface and cross-sectional morphologies and compositions of corrosion products were analyzed by scanning electron

microscopy (SEM), energy dispersive x-ray spectroscopy (EDS), and Raman spectroscopy. In addition, high resolution transmission electron microscopy (TEM) and EDS elemental mapping were performed on the cross-section of specimen with corrosion product layers formed on the surface.

3. Results

3.1. Comprehensive condition (Experiment 1)

The first experiment was conducted in so-called comprehensive condition which was derived from a process simulation close to the condition of a real gasification plant and contained all the corrosive species; CO_2 , H_2S , and $HCOOH$. The results of corrosion rate and OCP measurements for this condition are shown in Fig. 2.

According to Fig. 2, the initial corrosion rates are significantly high with a maximum rate of ~ 15 mm/y due to the high temperature. The corrosion rate then decreases and after 20 h and it stabilizes at a rate of ~ 1 mm/y until the end of the experiment. The OCP shows a similar trend to the corrosion rate as it decreases from -0.40 V to -0.55 V. Considering the solution chemistry and temperature, it is expected for iron sulfide (FeS) and/or magnetite (Fe_3O_4) to form which could provide a good protection to carbon steel. However, the final corrosion rate (~ 1 mm/y) does not reflect the expected protectiveness from these corrosion products.

The results of surface and cross-sectional characterizations using SEM, and EDS elemental mapping are shown in Fig. 3 and Fig. 4, respectively. According to Fig. 3(a), the surface of the specimen is fully covered by corrosion product that appears to have a morphology commonly observed for FeS [18,22]. The cross-section of this specimen shows a homogenous and seemingly single layered of corrosion product with a thickness of ~ 20 μm (Fig. 3(b)). However, according to the O mapping in Fig. 4(c), a thin layer of oxide is present at the interface of the specimen and the thick layer of FeS (see S mapping in Fig. 4 [b]). As it also appears from the O map, the oxide layer is not continuous, and its

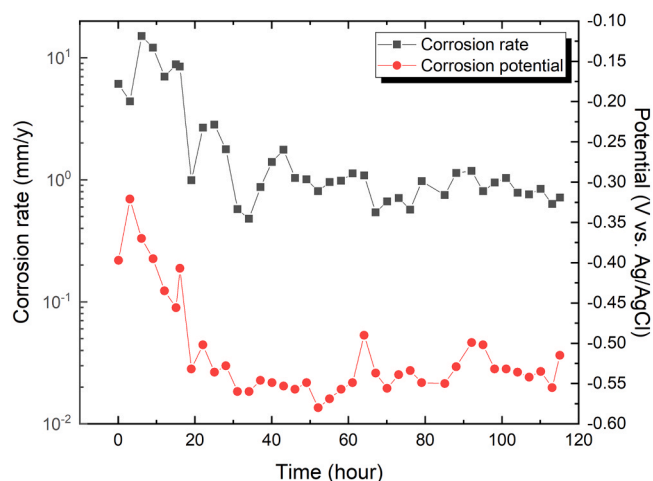


Fig. 2. Variations of corrosion rate and OCP with time for A106 steel specimen exposed to $CO_2/H_2S/HCOOH$ environment at 237 °C (Experiment 1).

Table 2
Experimental conditions for different tests.

Experiment ID	Temperature (°C)	pCO ₂ (MPa)	pH ₂ S (MPa)	HCOOH (M)	NaCl (wt%)	rotation (rpm)	pH	Duration (day)
1	237	0.115	0.024	0.082	-	510	5.3	5
2	237	0.115	-	0.082	-	510	5.3	3
3	237	0.115	-	-	-	510	5.3	3
4	237	0.115	-	-	1	510	5.3	2

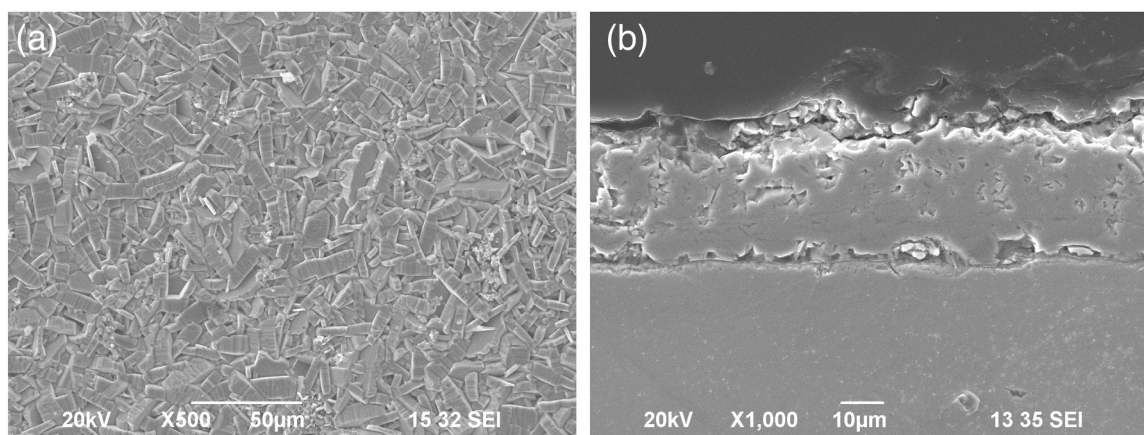


Fig. 3. SEM image of (a) surface and (b) cross-section of A106 steel specimen exposed to $CO_2/H_2S/HCOOH$ environment at 237 °C (Experiment 1).

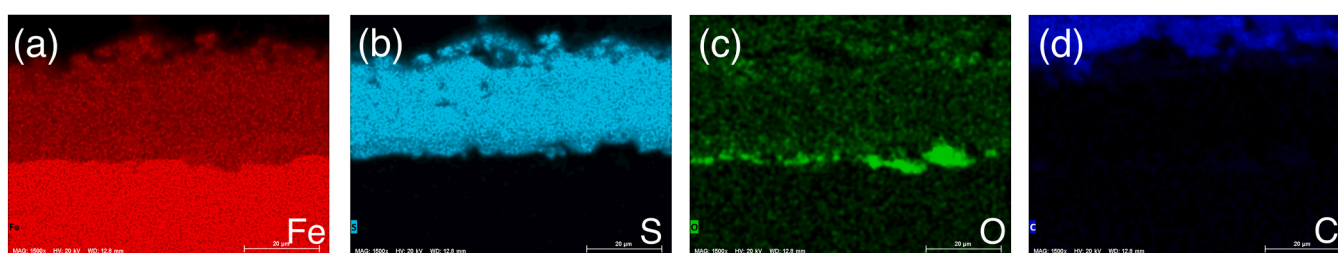


Fig. 4. Elemental mapping of (a) Fe, (b) S, (c) O, and (d) C across the cross-section shown in Fig. 3(b).

thickness might vary along the interface.

In order to confirm the composition of this duplex corrosion product layer, further phase characterizations on the surface and the cross-section of the specimen were carried out. The result of Raman spectroscopy of the corroded surface is presented in Fig. 5. The spectrum in this figure gives information about the top layer of the corrosion product and shows that it consists of pyrrhotite [33].

High resolution TEM image and the elemental mapping of the thin oxide layer are presented in Fig. 6. According to this figure, the thickness of the layer is around 1 µm. Since the TEM image shows a very small portion of the cross-section, it is not possible to determine the level of coverage of the entire surface by this inner layer. The high-resolution map in Fig. 6, clearly shows the distribution of oxygen across the thin inner layer, while S and C are absent from this layer. As expected, the

outer layer is rich in S.

The diffraction pattern was collected from the inner oxide layer and is shown in Fig. 7. The lattice spacing was determined by measuring the distance from the center of the pattern (its estimated location) to each ring or reflection that would indicate the location where a ring would be formed. This distance represents a lattice spacing in $1/d$. These measured spacings were compared to those of the various candidate crystals ($FeO(OH)$, Fe_2O_3 , Fe_3O_4 , etc.). Without an internal standard to calibrate the measurements we would expect ~5% error, therefore, the values may not match the tabulated values perfectly. This was corrected by applying a correction factor (scaling) to the measurements. From Table 3, the measured d-spacings mainly show correspondents with the tabulated values of Fe_3O_4 meaning that this layer is primarily made of magnetite. Some $FeO(OH)$ and Fe_2O_3 are also detected in this thin layer.

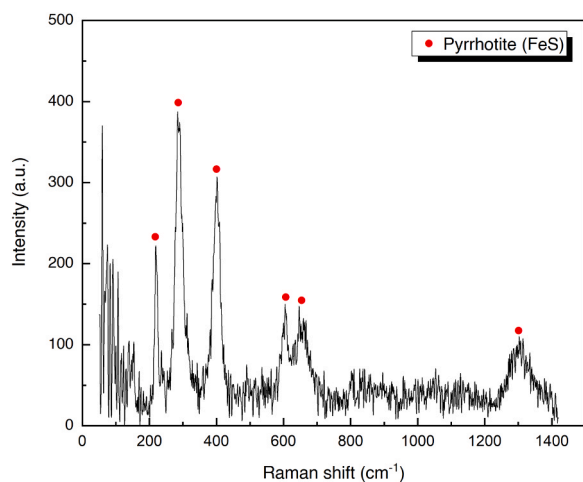


Fig. 5. Raman spectrum of A106 steel specimen exposed to $CO_2/H_2S/HCOOH$ environment at 237 °C (Experiment 1).

3.2. Effect of H_2S (Experiment 2)

As shown in the results of the experiment 1, the corrosion rate was ~ 1 mm/y with local formation of Fe_3O_4 . This corrosion rate is higher compared to the results of high temperature corrosion experiments in the existing literature when Fe_3O_4 is formed [14,16,21]. Thus, in order to investigate which specie(s) affect the formation of Fe_3O_4 , H_2S was eliminated from the system and the experiment was conducted under the same condition of Experiment 1. The results of corrosion rate and OCP measurements for this experiment are shown in Fig. 8. According to this figure, the corrosion rate starts with a lower value of ~2 mm/y, however, it follows a similar trend to that under the comprehensive condition (Fig. 2). A decrease in the corrosion rate is observed after ~10 h, followed by some fluctuations and a relatively stable rate at the end of experiment. The final corrosion rate at the end of this experiment is ~ 1 mm/y. The OCP changes in the range of -0.46 V to ~ -0.58 V during the experiment which is similar to the OCP changes in Experiment 1. The similar final corrosion rates between this condition and the comprehensive condition imply that H_2S is not the main corrosive specie that results in the high corrosion rate in this system.

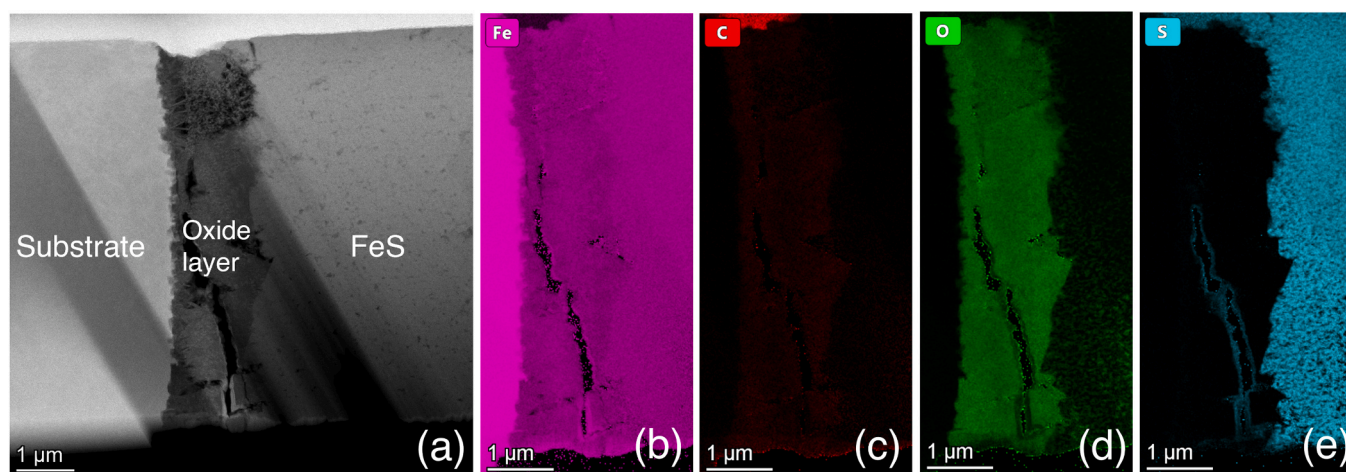


Fig. 6. (a) TEM high resolution image and elemental mapping of (b) Fe, (c) C, (d) O, and (e) S of A106 steel specimen exposed to $CO_2/H_2S/HCOOH$ environment at 237 °C (Experiment 1).

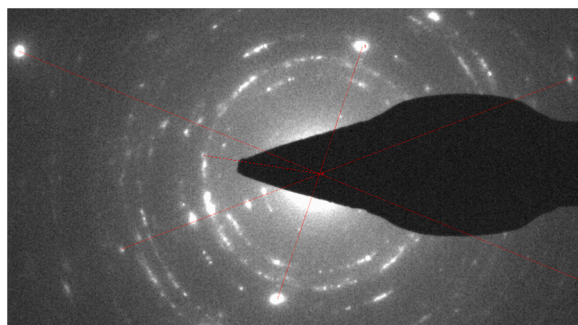


Fig. 7. Diffraction pattern of the inner corrosion product layer (indicated in Fig. 6 as oxide layer) on A106 steel specimen exposed to $CO_2/H_2S/HCOOH$ environment at 237 °C (Experiment 1).

Table 3
Analysis of the diffraction pattern shown in Fig. 7.

1/d (nm ⁻¹)	Phase
3.37	Fe_3O_4
3.44	Fe_3O_4
2.08	Fe_3O_4
1.99	$FeO(OH)$
2.67	Fe_2O_3
3.95	Fe_3O_4
3.40	Fe_3O_4
4.81	Fe_3O_4
6.20	Fe_3O_4
4.00	Fe_2O_3
4.07	Fe_3O_4

The results of SEM analysis of the surface and cross-section of the specimen after Experiment 2 are shown in Fig. 9. It can be seen that a relatively thin corrosion product layer is formed under this condition with a smooth surface morphology. Some cracks are observed on the surface and the cross-sectional view, which reveal that the layer is discontinuous and apparently non-adherent. The results of elemental mapping in Fig. 10 shows the presence of Fe and O in this layer.

The absence of FeS layer, as a result of eliminating H_2S from the system, even as a compact layer such as the one shown in Fig. 3(b), made no difference in the corrosion rate, meaning that it is not the main protective element in the corrosion product layer.

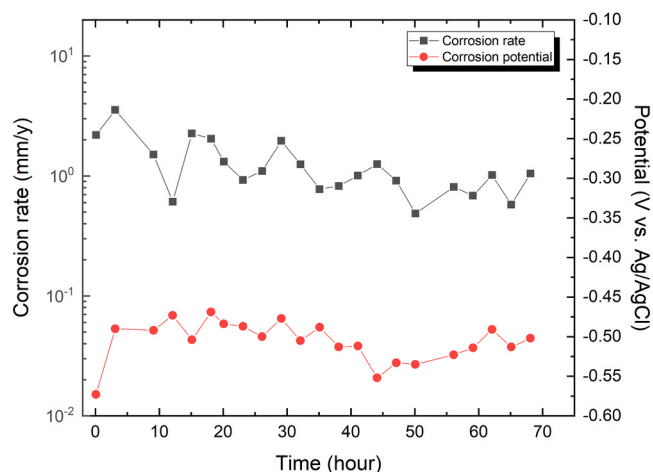


Fig. 8. Variations of corrosion rate and OCP with time for A106 steel specimen exposed to $CO_2/HCOOH$ environment at 237 °C (Experiment 2).

3.3. Effect of HCOOH (Experiment 3)

In the next step of the investigation, $HCOOH$ was also excluded from the solution, in addition to H_2S . At the beginning of this experiment, the same pH value (5.3) was adjusted by adding HCl to the solution. As explained earlier in detail, the pH value was calculated based on the water chemistry model presented in another publication [5]. The results of corrosion rate and OCP measurements during this experiment are depicted in Fig. 11.

As shown in Fig. 11, in the absence of $HCOOH$ and H_2S , the corrosion starts at a rate of ~1.6 mm/y followed by a sharp decline in less than 10 h. The decrease in the corrosion rate continues until ~50 h after which some resemblance of a plateau is reached. The final corrosion rate (0.06 mm/y) achieved here is significantly lower compared to the two previous conditions that contained $HCOOH$. Another significant difference between the results of this condition and those of the previous ones, is the range of OCP (−0.25 V to −0.35 V) which is more noble compared to those measured during Experiments 1 and 2 (with a range of −0.50 V to −0.58 V). The measured low corrosion rate with a nobler OCP in the condition without $HCOOH$ indicates that the anodic reaction is suppressed by the formation of a protective corrosion product layer.

The SEM images of the surface and cross-section of the specimen after this experiment are shown in Fig. 12. The surface and cross-sectional morphologies of the corrosion product is similar to that

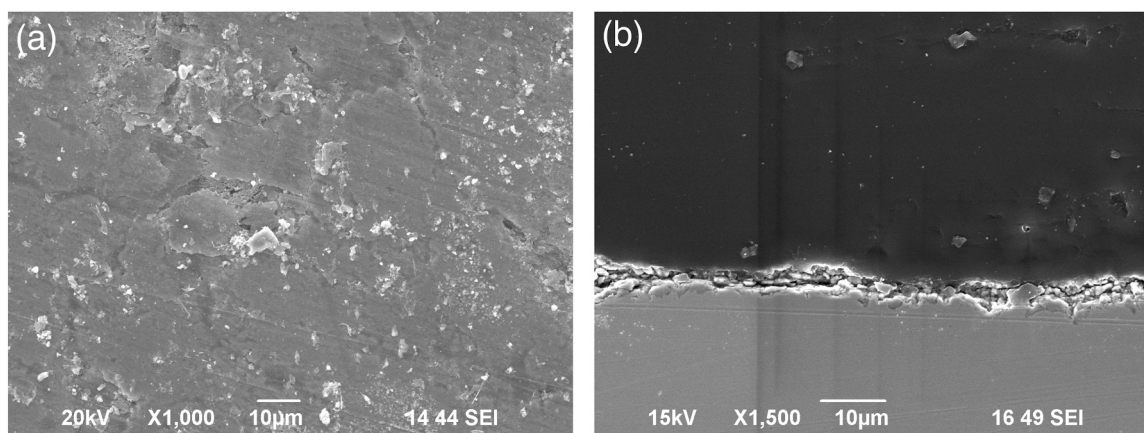


Fig. 9. SEM image of (a) the surface and (b) the cross-section of A106 steel specimen exposed to $CO_2/HCOOH$ environment at 237 °C (Experiment 2).

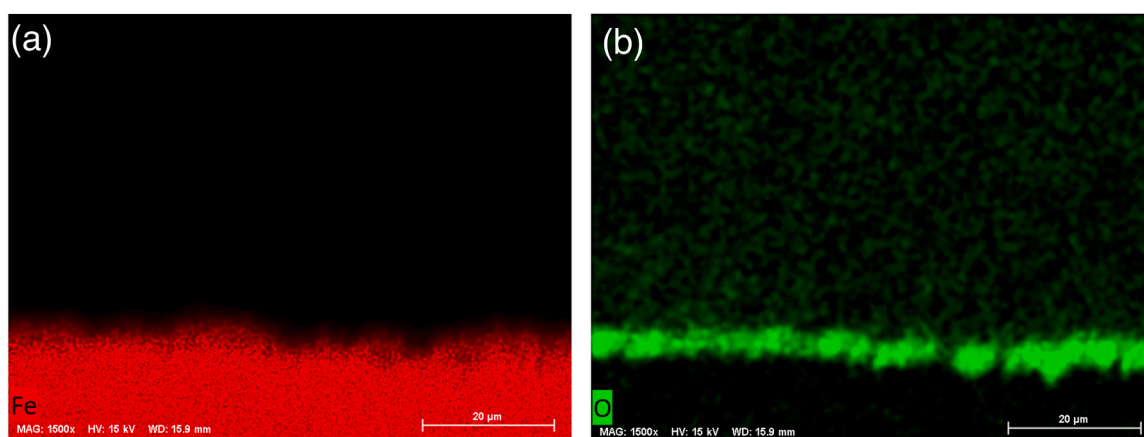


Fig. 10. Elemental mapping of (a) Fe and (b) O across the cross-section shown in Fig. 9(b).

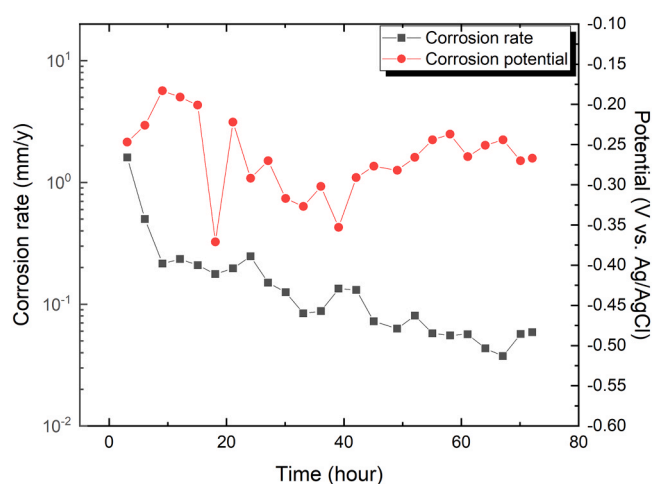


Fig. 11. Variations of corrosion rate and OCP with time for A106 steel specimen exposed to CO_2 environment at 237 °C (Experiment 3).

formed in the condition without H_2S (Fig. 9 and Fig. 10, Experiment 2). However, as shown in the cross-sectional image, the layer seems to be compact and adherent to the steel substrate which could be the reason for the low corrosion rate under this condition. The results of the elemental mapping for the cross-sectional view show that the corrosion product layer contains Fe and O (Fig. 13).

Raman spectroscopy analysis on the surface of the specimen (Fig. 14)

identifies the corrosion product layer as Fe_3O_4 . The surface of the specimen contains some hematite Fe_2O_3 as well, which might have formed due to oxidation of the specimen during storage period.

In order to confirm the effect of $HCOOH$, a reference experiment was performed in a CO_2 containing 1 wt% $NaCl$ solution at the same pH of 5.3. The choice of 1 wt% $NaCl$ solution is to have a solution with enough conductivity to perform electrochemical measurements without having any major effect on the corrosion or the formation of corrosion product layers. The results of corrosion rate and OCP measurements during this experiment are shown in Fig. 15. According to this figure, a sharp decrease in the corrosion rate from ~ 1.8 mm/y to 0.06 mm/y occurs in less than 10 h. This low corrosion rate remains almost constant until the end of the experiment after 40 h. In this case the protective corrosion product layer readily starts to form in a short period of time, similar to what was observed in the experiment without $HCOOH$ (Fig. 11, Experiment 3). The corresponding increase in OCP toward more noble values confirms this.

SEM images of the surface and cross-section of the specimen after this experiment are presented in Fig. 16. These images show a homogeneous corrosion product layer, with a thickness of ~ 10 μm on the specimen. Some powder-like corrosion products are also observed on top of the main corrosion product layer, which do not play any role in corrosion protection. The results of EDS elemental mapping in Fig. 17 show the presence of O and Fe across the main corrosion product layer. Using Raman spectroscopy, the composition of this layer was confirmed to be Fe_3O_4 (the results are not shown here).

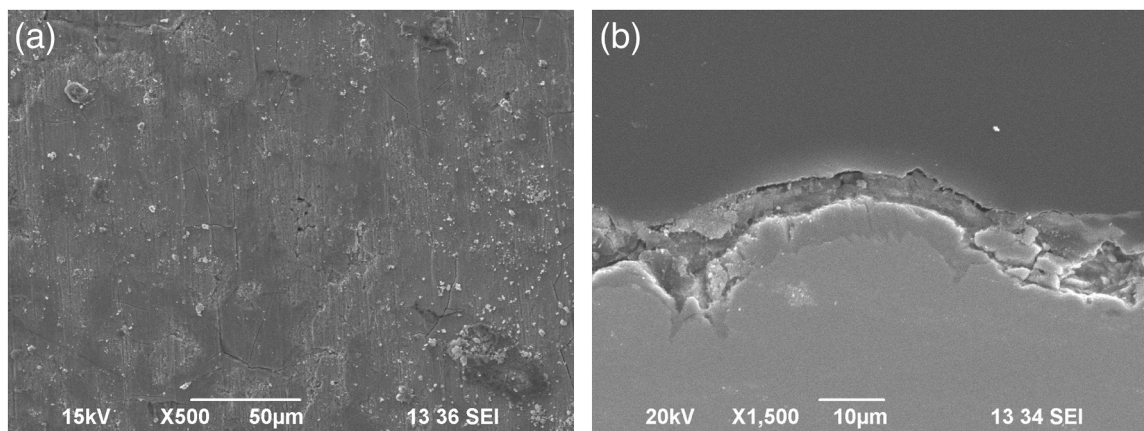


Fig. 12. SEM image of (a) the surface and (b) the cross-section of A106 steel specimen exposed to CO_2 environment at 237°C (Experiment 3).

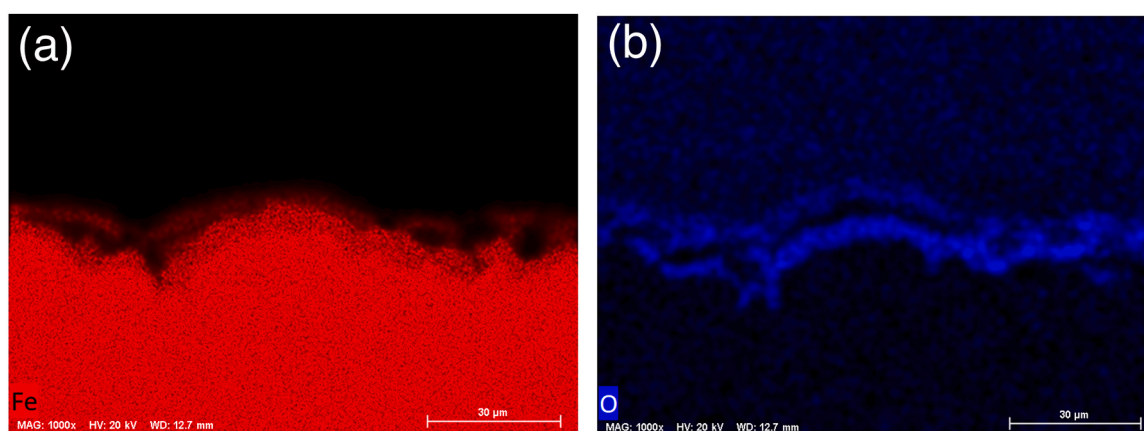


Fig. 13. Elemental mapping of (a) Fe and (b) O across the cross-section shown in Fig. 12 (b).

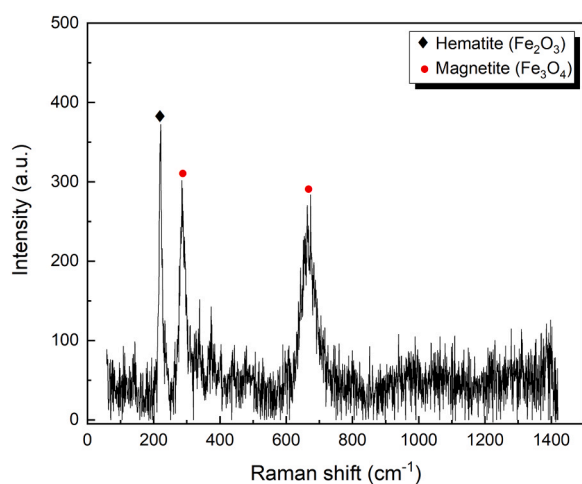


Fig. 14. Raman spectrum of the surface of A106 steel specimen exposed to CO_2 environment at 237°C (Experiment 3).

4. Discussion

The corrosion rate of carbon steel in the comprehensive condition which contained all possible corrosive species (CO_2 , H_2S , and HCOOH) was measured to be about 1 mm/y (Fig. 2). Formation of Fe_3O_4 layer [14,16,21] is expected to decrease this rate. However, as shown in Fig. 3 to Fig. 6, at this condition a thin and discontinuous Fe_3O_4 layer was

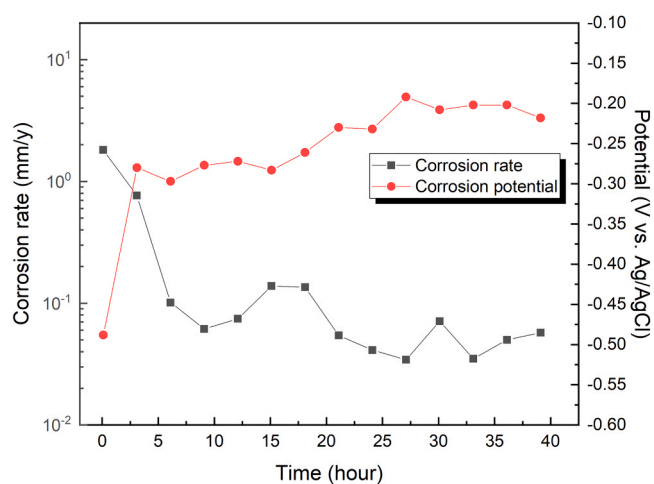


Fig. 15. Variations of corrosion rate and OCP with time for A106 steel specimen exposed to CO_2/NaCl environment at 237°C (Experiment 4).

formed, which does not provide sufficient protection. A parametric study was conducted to discover which corrosive specie(s) interfere with the formation of Fe_3O_4 . Fig. 18 presents a comparison of the corrosion rates at different conditions evaluated in the present study. It can be seen that the corrosion rates of the conditions in which HCOOH is present, are about one order of magnitude higher than those of the other cases. According to the results of cross-sectional analysis shown above, Fe_3O_4 is

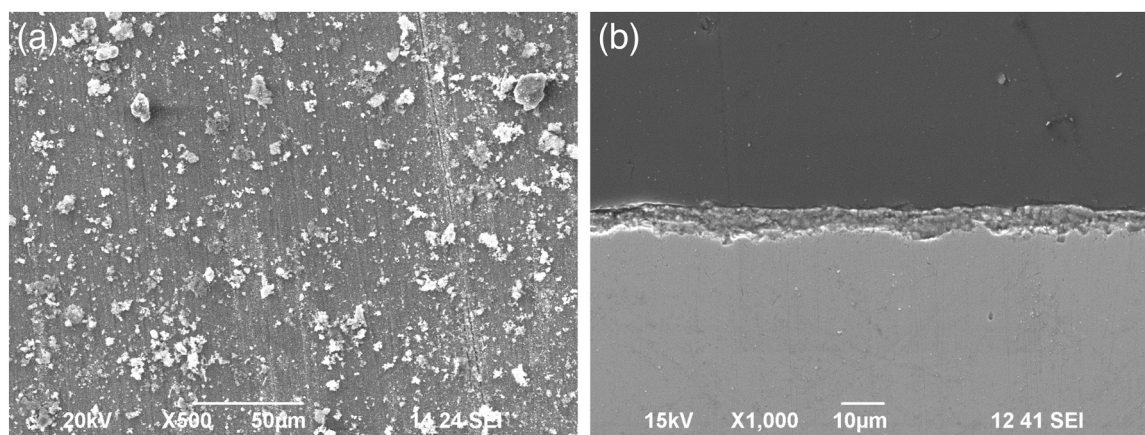


Fig. 16. SEM image of (a) the surface and (b) the cross-section of A106 steel specimen exposed to $CO_2/NaCl$ environment at $237^\circ C$ (Experiment 4).

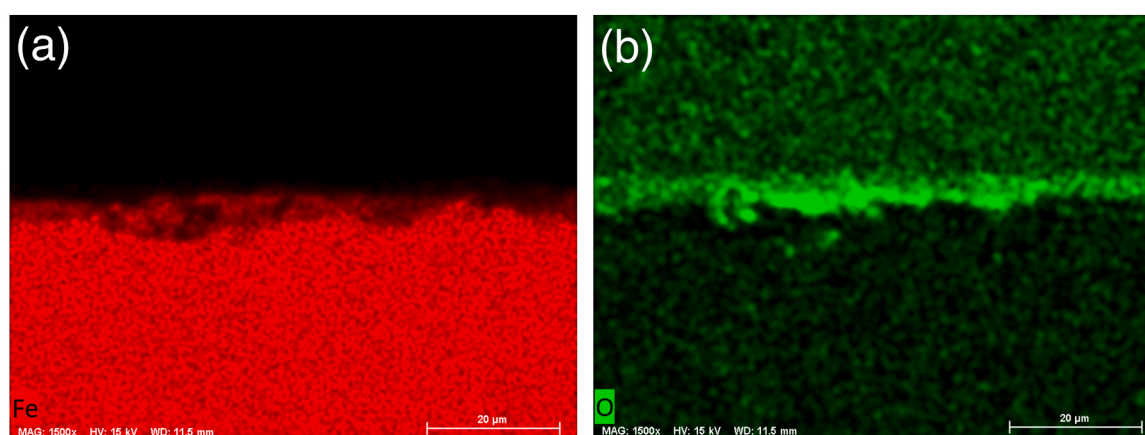


Fig. 17. Elemental mapping of (a) Fe and (b) O across the cross-section shown in Fig. 16 (b).

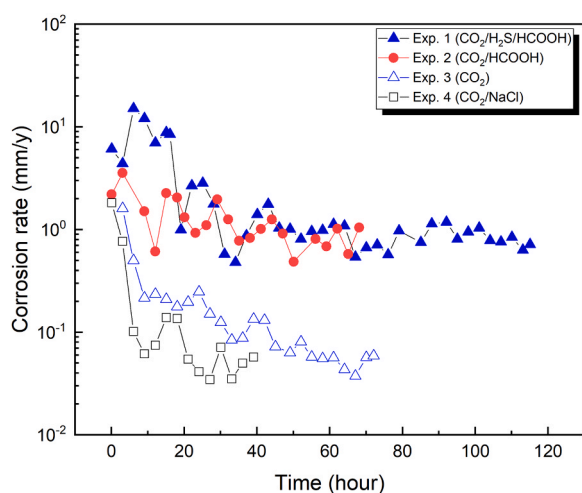


Fig. 18. Comparison of corrosion rate measurements during different experiments.

not sufficiently formed in the presence of $HCOOH$.

To confirm this effect of $HCOOH$ on the formation of Fe_3O_4 , another experiment was conducted in the absence of $HCOOH$ but in the presence of H_2S in the system. The cross-sectional SEM image and the elemental mapping of the specimen after this experiment are shown in Fig. 19. This image and the distribution of Fe, O and S clearly indicate a corrosion

product layer with a duplex structure consisting of the inner layer (containing Fe and O) and the outer layer (containing Fe and S). Raman spectroscopy measurement was carried out on this inner layer (shown in Fig. 20) which was proved to be Fe_3O_4 . The corrosion rate measured in this condition was similar to those monitored in the cases without $HCOOH$. This confirms that Fe_3O_4 can form at high temperature in the absence of $HCOOH$, and provides sufficient protection to carbon steel.

The overall results show that in the studied system, the presence of the Fe_3O_4 layer can result in a low corrosion rate (< 0.1 mm/y) if its formation and/or integrity are not compromised by some of the chemicals in the environment. The results also indicate that $HCOOH$ is the main corrosive specie increasing the corrosion rate due to its interference with the formation of the protective Fe_3O_4 layer. In order to explain this behavior, we need to look at the thermodynamics of corrosion product layer formation in this system.

Pourbaix diagrams for the comprehensive condition with and without H_2S in the system (corresponding to Experiments 1 and 2) are shown in Fig. 21. Details of construction of such diagrams for $Fe-H_2S-H_2O$ and $Fe-CO_2-H_2O$ systems were investigated by Ning [34] and Tanupabrungsun et al. [14], respectively. According to Fig. 21 (a), at pH 5.3 and potential of $-0.5 V_{SHE}$, with H_2S present in the system, FeS (pyrrhotite) is the most thermodynamically stable corrosion product. In the absence of H_2S , Fe_3O_4 is the most stable phase (Fig. 21 (b)). While our results that showed the precipitation of Fe_3O_4 as the main phase under the experimental conditions without H_2S (Experiments 2 ~ 4) agree with the thermodynamic data shown in Fig. 21 (b), the experimental results obtained from the conditions with H_2S (when the formation of Fe_3O_4 is not thermodynamically expected but we observed

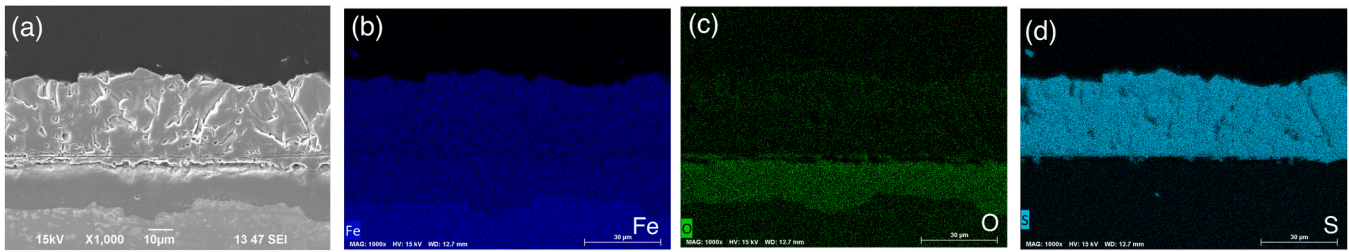


Fig. 19. SEM image of (a) the cross-section of A106 steel specimen exposed to CO_2/H_2S environment at 237 °C. Elemental mapping of (b) Fe, (c) O and (d) S across the cross-section shown in Fig. 18 (a).

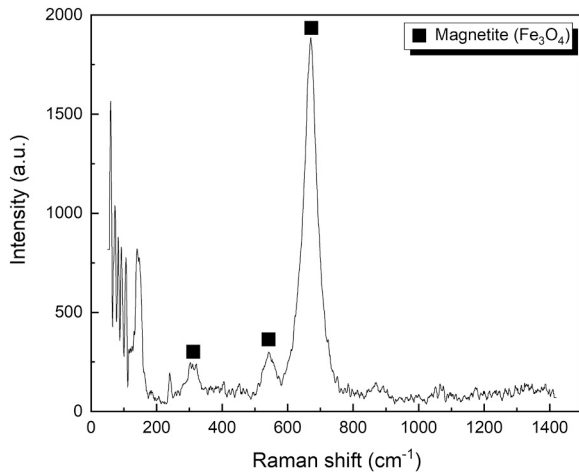


Fig. 20. Raman spectrum of the inner corrosion product layer on A106 steel specimen exposed to CO_2/H_2S environment at 237 °C.

it from the experiment) apparently do not match with the thermodynamic data (Fig. 21 (a)). This indicates that Fe_3O_4 is kinetically favored at high temperatures as a part of the corrosion product layer near the metal surface in the presence of H_2S .

Even though it is proven that both FeS and Fe_3O_4 can be formed in the current experimental conditions in the presence of H_2S , the question remains as why the presence of $HCOOH$ interferes with the formation of the protective Fe_3O_4 layer?

The precipitation of Fe_3O_4 and FeS is thermodynamically possible when their saturation value is above unity (also called supersaturation, $S_{Fe_3O_4}$ and S_{FeS}). However, research has shown that in the presence of organic acids (such as CH_3COOH) in the system, the formation of ferrous

complexes could possibly decrease these supersaturation values. As an example, Fajardo *et al.* [31] suggested that the formation of ferrous complexes such as ferrous acetate could cause the partial dissolution of $FeCO_3$ layer, therefore, one plausible mechanism is to assume that similar ferrous complexes can form in the presence of formate ($COOH^-$):



Formation of ferrous formate ($Fe(COOH)^+$) in the presence of $HCOOH$ has been indeed observed and reported by other researchers [35]. In this case, if Fe^{2+} ions are bonded to $COOH^-$, the concentration of Fe^{2+} available to form Fe_3O_4 or FeS decreases, i.e. $S_{Fe_3O_4}$ and S_{FeS} decrease. However, according to the results of Experiment 1 (Fig. 3), formation of such complexes apparently has no influence on the formation of FeS , however, it possibly interferes with the formation of Fe_3O_4 . The reason for this difference could be due to differences in the rate of formation of FeS , $Fe(COOH)^+$, and Fe_3O_4 . If we assume that FeS possibly has the fastest formation kinetics and Fe_3O_4 has the slowest formation rate, it is reasonable to postulate that the formation of $Fe(COOH)^+$ impedes the formation of Fe_3O_4 and not FeS . While FeS forms faster and at the initial stage of the corrosion process, Fe_3O_4 requires more time to form and even then, its formation could be slower than $Fe(COOH)^+$. Therefore, in the presence of $HCOOH$, at the FeS /metal interface, Fe^{2+} ions are bonded to $COOH^-$ which hinders (at least partially) the formation of a protective Fe_3O_4 layer. This conclusion is, however, not definitive. Further investigation is needed to understand the exact mechanism of unfavorable effect of $HCOOH$ on Fe_3O_4 formation.

5. Conclusions

- The following conclusions can be drawn from this study:
- The corrosion rate of carbon steel under the gasification plant environment containing CO_2 , H_2S , and $HCOOH$ was relatively high

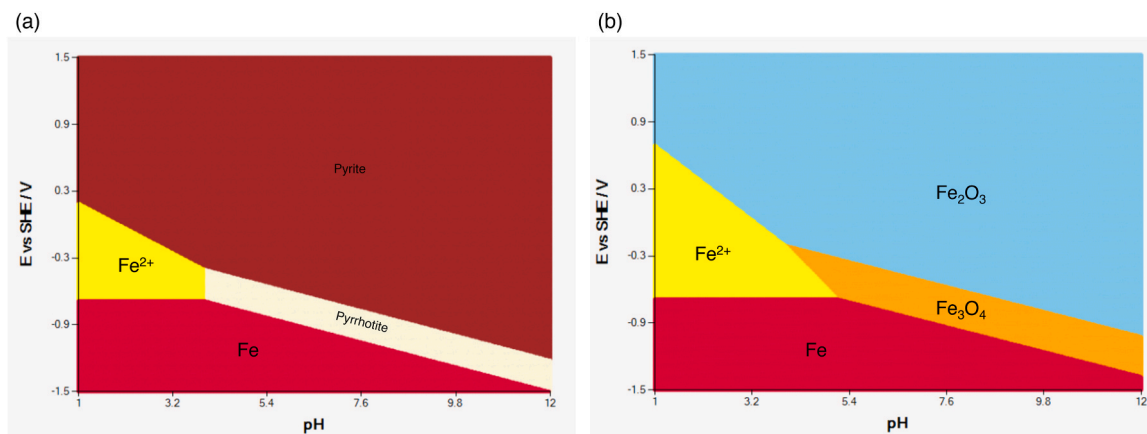


Fig. 21. Generated Pourbaix diagrams for (a) $Fe-CO_2-H_2S-H_2O$ and (b) $Fe-CO_2-H_2O$ systems corresponding to the comprehensive condition (237 °C, 0.115 MPa pCO_2 , and 0.024 MPa pH_2S , with arbitrary $c_{Fe^{2+}}$: 10 ppm, $c_{Fe^{3+}}$: 1 ppm).

(~ 1 mm/y) because Fe_3O_4 , which is generally known to be protective in high temperature corrosion, was not sufficiently formed.

- As a result of the parametric study, it was found that $HCOOH$ present in the solution interfered with the formation of Fe_3O_4 , and FeS alone cannot provide sufficient protection.
- The exact mechanism of how the presence of $HCOOH$ hinders the formation of Fe_3O_4 was not revealed in this study, but it is probably because the complex formation with Fe and $HCOOH$ is promoted at high temperature and the Fe^{2+} ions necessary for the formation of Fe_3O_4 are insufficient due to the complexes.

CRedit authorship contribution statement

Breining Robert: Writing – review & editing, Conceptualization. **Nesic Srdjan:** Writing – review & editing, Supervision, Funding acquisition. **Eslami Maryam:** Writing – original draft, Methodology, Investigation, Data curation. **Choi Yoon-Seok:** Writing – review & editing, Supervision, Data curation, Conceptualization.

Declaration of Competing Interest

The authors declare that they have no known competing financial interests or personal relationships that could have appeared to influence the work reported in this paper.

Data availability

Data will be made available on request.

Acknowledgements

The authors would like to acknowledge the funding support of this research from Air Liquide Global E&C Solution.

References

- [1] T. Tiernan, K. Natesan, Metallic corrosion in simulated low-Btu coal-gasification atmospheres, *J. Mater. Energy Syst.* 1 (1980) 13–29.
- [2] K. Natesan, High-temperature corrosion in coal gasification systems, *Corrosion* 41 (1985) 646–655.
- [3] G. Wire, E. Vesely, S. Agarwal, Erosion-corrosion of metals in coal gasification atmospheres, *J. Mater. Energy Syst.* 8 (1986) 150–167.
- [4] W. Debruyne, F. Casteels, H. Tas, Corrosion of materials in an environment typical of coal gasification plants, *Mater. Sci. Eng.* 87 (1987) 169–174.
- [5] M. Nordsveen, S. Nešić, R. Nyborg, A. Stangeland, A mechanistic model for carbon dioxide corrosion of mild steel in the presence of protective iron carbonate films—Part 1: theory and verification, *Corrosion* 59 (2003) 443–456.
- [6] X. Wen, P. Bai, B. Luo, S. Zheng, C. Chen, Review of recent progress in the study of corrosion products of steels in a hydrogen sulphide environment, *Corros. Sci.* 139 (2018) 124–140.
- [7] S.N. Smith, Current understanding of corrosion mechanisms due to H₂S in oil and gas production environments, in: *Corrosion, NACE International*, Dallas, Texas, 2015, paper no. 5485.
- [8] K. Natesan, Corrosion-erosion behavior of materials in a coal-gasification environment, *Corrosion* 32 (1976) 364–370.
- [9] J.L.J. Soler, D.J. Baxter, J.F. Norton, Effects of silicon and titanium on the corrosion of low-alloy steels in a simulated coal gasification environment at 600°C, *Corrosion* 55 (1999) 1191–1200.
- [10] S. Lee, S.-W. Chung, S.-J. Lee, Y. Yun, Corrosion of type 316L stainless steel piping in synthetic gas plants, *Corrosion* 69 (2013) 921–953.
- [11] N. Mundhenk, S. Carrero, K.G. Knauss, R. Wonneberger, A. Undisz, Y. Wu, Kinetic and thermodynamic analysis of high-temperature CO₂ corrosion of carbon steel in simulated geothermal NaCl fluids, *Corros. Sci.* (2020) 108597.
- [12] V. Srinivasan, R.A. Padgett Jr., A. Choudhury, Sulfidation behavior of Fe-25Cr-20Ni-3Si in H₂/H₂O/H₂S/Ar at 700°C, *Corrosion* 47 (1991) 703–712.
- [13] Z.F. Yin, Y.R. Feng, W.Z. Zhao, Z.Q. Bai, G.F. Lin, Effect of temperature on CO₂ corrosion of carbon steel, *Surf. Interface Anal.* 41 (2009) 517–523.
- [14] T. Tanupabrungrun, D. Young, B. Brown, S. Nešić, Construction and verification of pourbaix diagrams for CO₂ corrosion of mild steel valid up to 250 °C, in: *Corrosion, NACE International*, Salt Lake City, Utah, 2012, paper no. 1418.
- [15] N. Mundhenk, K.G. Knauss, S.R.S. Bandaru, R. Wonneberger, T.M. Devine, Corrosion of carbon steel and the passivating properties of corrosion films formed under high-PT geothermal conditions, *Sci. Total Environ.* 677 (2019) 307–314.
- [16] Y. Hua, S. Xu, Y. Wang, W. Taleb, J. Sun, L. Zhang, R. Barker, A. Neville, The formation of FeCO₃ and Fe₃O₄ on carbon steel and their protective capabilities against CO₂ corrosion at elevated temperature and pressure, *Corros. Sci.* 157 (2019) 392–405.
- [17] S. Gao, P. Jin, B. Brown, D. Young, S. Nešić, M. Singer, Effect of high temperature on the aqueous H₂S corrosion of mild steel, *Corrosion* 73 (2017) 1188–1191.
- [18] S. Gao, P. Jin, B. Brown, D. Young, S. Nešić, M. Singer, Corrosion behavior of mild steel in sour environments at elevated temperatures, *Corrosion* 73 (2017) 915–926.
- [19] T.A. Ramanarayanan, S.N. Smith, Corrosion of iron in gaseous environments and in gas-saturated aqueous environments, *Corrosion* 46 (1990) 66–74.
- [20] J. Kvarekval, R. Nyborg, H. Choi, Formation of multilayer iron sulfide films during high temperature CO₂/H₂S corrosion of carbon steel, in: *Corrosion, NACE International*, San Diego, California, 2003, paper no. 03339.
- [21] Shujun Gao, B. Brown, D. Young, S. Nešić, M. Singer, Formation mechanisms of iron oxide and iron sulfide at high temperature in aqueous H₂S corrosion environment, *J. Electrochem. Soc.* 165 (2018) C171–C179.
- [22] S. Gao, B. Brown, D. Young, M. Singer, Formation of iron oxide and iron sulfide at high temperature and their effects on corrosion, *Corros. Sci.* 135 (2018) 167–176.
- [23] I. Sekine, K. Senoo, The corrosion behaviour of SS 41 steel in formic and acetic acids, *Corros. Sci.* 24 (1984) 439–448.
- [24] I. Sekine, S. Hatakeyama, Y. Nakazawa, Effect of water content on the corrosion behaviour of type 430 stainless steel in formic and acetic acids, *Electrochim. Acta* 32 (1987) 915–920.
- [25] I. Sekine, K. Momoi, Corrosion behavior of SUS 329J1 stainless steel in formic acid solution, *Corrosion* 44 (1988) 136–142.
- [26] E. Otero, A. Pardo, M.V. Utrilla, F.J. Pérez, C. Merino, The corrosion behaviour of AISI 304L AND 316L stainless steels prepared by powder metallurgy in the presence of organic acids, *Corros. Sci.* 39 (1997) 453–463.
- [27] A.J. Invernizzi, E. Sivieri, S.P. Trasatti, Corrosion behaviour of Duplex stainless steels in organic acid aqueous solutions, *Mater. Sci. Eng. A* 485 (2008) 234–242.
- [28] S.K. Singh, A.K. Mukherjee, M.M. Singh, Kinetics of mild steel corrosion in aqueous formic acid solutions, *Can. Metall. Q.* 50 (2011) 186–194.
- [29] G.E. Badea, D. Ionita, P. Cret, Corrosion and passivation of the 304 stainless steel in formic acid solutions, *Mater. Corros.* 65 (2014) 1103–1110.
- [30] V. Fajardo, C. Canto, B. Brown, S. Nešić, Effect of Organic Acids in CO₂ Corrosion, in: *Corrosion, NACE International*, Nashville, TN, 2007, paper no. 07319.
- [31] V. Fajardo, M. Eslami, Y.-S. Choi, B. Brown, S. Nešić, Influence of acetic acid on the integrity and protectiveness by an iron carbonate (FeCO₃) corrosion product layer, *Corrosion* 77 (2021) 97–111.
- [32] S. Nešić, G.T. Solvi, S. Skjerve, Comparison of rotating cylinder and loop methods for testing CO₂ corrosion inhibitors, *Br. Corros. J.* 32 (1997) 269–276.
- [33] I. Weber, U. Böttger, S.G. Pavlov, H.-W. Hübers, H. Hiesinger, E.K. Jessberger, Laser alteration on iron sulfides under various environmental conditions, *J. Raman Spectrosc.* 48 (2017) 1509–1517.
- [34] J. Ning, The role of iron sulfide polymorphism in localized corrosion of mild steel, PhD Dissertation, Ohio University, 2016.
- [35] R.M. Connatser, S.A. Lewis, J.R. Keiser, J.-S. Choi, Measuring bio-oil upgrade intermediates and corrosive species with polarity-matched analytical approaches, *Biomass Bioenergy* 70 (2014) 557–563.